



Cite this: DOI: 10.1039/c4nr04485a

A high transmission wave-guide wire network made by self-assembly

Stefano Salvatore,^a Silvia Vignolini,^b Julian Philpott,^a Morgan Stefik,^c Ulrich Wiesner,^c Jeremy J. Baumberg^a and Ullrich Steiner^{*a,d}

Polymer self-assembly of a 3D continuous gyroid morphology was replicated into a network consisting of hollow gold struts. This was achieved by first replicating a gyroid structured film into nickel. The Ni network was employed as an electrode for electrochemical Au deposition, followed by the removal of Ni. The resulting hollow network of plasmonic gold exhibited a substantial optical transmission enhancement by a factor of nearly 3, compared to a network of full Au struts. The overall transmission across the hollow wave-guide morphology depends sensitively on the wall-thickness of the hollow struts down to 1 nm. The dramatic transmission increase arises from an interplay of three mechanisms: (1) the additional number of modes propagating through the wave-guide structure, (2) the increased efficiency of light in-coupling, and (3) a reduction of dissipation by decreasing the Au-volume experienced in plasmon mode propagation.

Received 5th August 2014,
Accepted 20th November 2014

DOI: 10.1039/c4nr04485a

www.rsc.org/nanoscale

1 Introduction

Optical metamaterials have recently received increasing attention, enabling fascinating and sought-after properties and functionalities such as negative refractive indices,^{1,2} super-lensing^{1,3} and cloaking devices.^{4,5} While there are now a large number of metamaterials that are active at microwave, terahertz and infrared frequencies,^{4,6–11} metamaterials for visible wavelengths are problematic because of their difficulty in fabrication and their high losses, which are the main obstacles towards their optical applications.¹² Reducing these losses to enable high optical transmission is therefore the key to design effective and functional optical metamaterials.

Optical metamaterials that are based on 3D sub-micrometer periodic lattices rely on the propagation of surface-plasmon polaritons across the network structure. These electron plasma oscillations are damped in the two materials adjacent to the interface. While the dissipation in one of these phases (air) is negligible, substantial losses occur in the metal that supports the plasmon resonance. The only way to solve this conundrum is by reducing the amount of the metal at the plasmonic inter-

face, similar to the utilisation of coaxial cables and wave-guides for high frequency signal transduction.

Here, we present an implementation of this approach by creating a three dimensional self-assembled metamaterial consisting of a hollow-wire-network that shows exceptionally high transmission and reduced absorption. This work is based on recent theoretical^{13,14} and experimental^{15,16} studies employing the gyroid morphology as a model system for 3D optical metamaterials. A negative refractive index at optical wavelengths has been predicted for this topology.¹⁷

Our approach is based on the self-assembly of block copolymers,¹⁸ consisting of two or more covalently tethered linear chains. Self-assembly in these systems is driven by microphase separation that balances the reduction of the free energy of mixing with the creation of unfavourable interfaces and chain stretching.¹⁹ This results in a large range of periodic 3D architectures controlled by the number of polymer blocks and their relative molecular weight.²⁰ Tri-block terpolymers with suitable block lengths can self-assemble into a double gyroid morphology, where each of the two gyroid networks and the surrounding matrix are chemically distinct. The removal of one gyroidal network and its replacement by gold gave rise to a chiral network morphology made of a plasmonic metal.¹⁵ The optical response of this nanoporous continuous strut-network showed a substantially reduced plasma frequency compared to solid gold, which arose from a combination of a reduction in the average electron density and an increased self-inductance of the highly interconnected and ordered network of the metal.^{15,16}

^aCavendish Laboratory, Department of Physics, University of Cambridge, J. J. Thomson Avenue, Cambridge CB3 0HE, UK. E-mail: ullrich.steiner@unifr.ch

^bDepartment of Chemistry, University of Cambridge, Lensfield Road, Cambridge CB2 1EW, UK

^cDepartment of Materials Science & Engineering, Cornell University, Ithaca, New York 14853, USA

^dAdolphe Merkle Institute, Chemin des Verdiers, CH-1700 Fribourg, Switzerland

2 Experimental

2.1. Sample fabrication

In this study, a polyisoprene-*block*-polystyrene-*block*-polyethylene oxide (ISO) terpolymer was used that assembles into two interpenetrating, chemically distinct gyroid networks (isoprene and ethylene oxide), which are embedded in a majority styrene phase. The ISO has an overall molecular weight of 33 kg mol^{-1} with relative volume fractions of 30% (isoprene), 53% (styrene) and 17% (ethylene oxide) that self-assembles upon annealing into a double gyroid morphology with a unit cell size of 35 nm. Several hundred nm-thick films were made by spin-coating followed by annealing for 20 min at 180 °C in a vacuum oven. The polyisoprene phase was selectively degraded by UV irradiation for two hours and rinsed away with ethanol. The resulting porous network was then back-filled with nickel by electrodeposition from a glass substrate coated with fluorinated tin oxide (FTO). In the electrochemical setup the FTO layer acted as a working electrode, a saturated calomel electrode was used as the reference electrode, and a platinum mesh acted as the counter electrode. The thickness of the deposit could be tuned by adjusting the electrodeposition duration and was set to $\sim 300 \text{ nm}$. The remaining polymers were subsequently removed by plasma etching, resulting in a free-standing Ni single gyroid (Fig. 1, top). This nickel structure

was then used as the working electrode for electrodeposition of gold, which deposits homogeneously around the Ni struts (Fig. 1, middle). In the final step, the inner nickel core is etched away by immersion in FeCl_3 , resulting in a hollow gyroid morphology (Fig. 1, bottom).

The nickel-plating solution was bought from Alfa Aesar (no. 42027), and the gold-plating solution was purchased from Technin (no. EC60) with 0.5 vol% brightener added to achieve a smooth deposition.

2.2. EDX characterization

EDX analysis was performed with a LEO GEMINI 1530VP FEG-SEM system that allows elemental analysis with a resolution of $<1\%$. The data were collected at 20 keV for 300 s. The measurements were performed on the bare Ni gyroid, after Au plating, and after Ni removal.

2.3. Optical characterization

A modified optical microscope equipped for spectroscopy was used to collect spectra. A 50 μm core optical fiber mounted in the conjugate plane of the focal plane of a 20 \times objective (NA = 0.24) served as a pinhole in the conjugate to the focal plane of the microscope objective, allowing us to collect spectra in a specific position. The halogen lamp of the microscope was

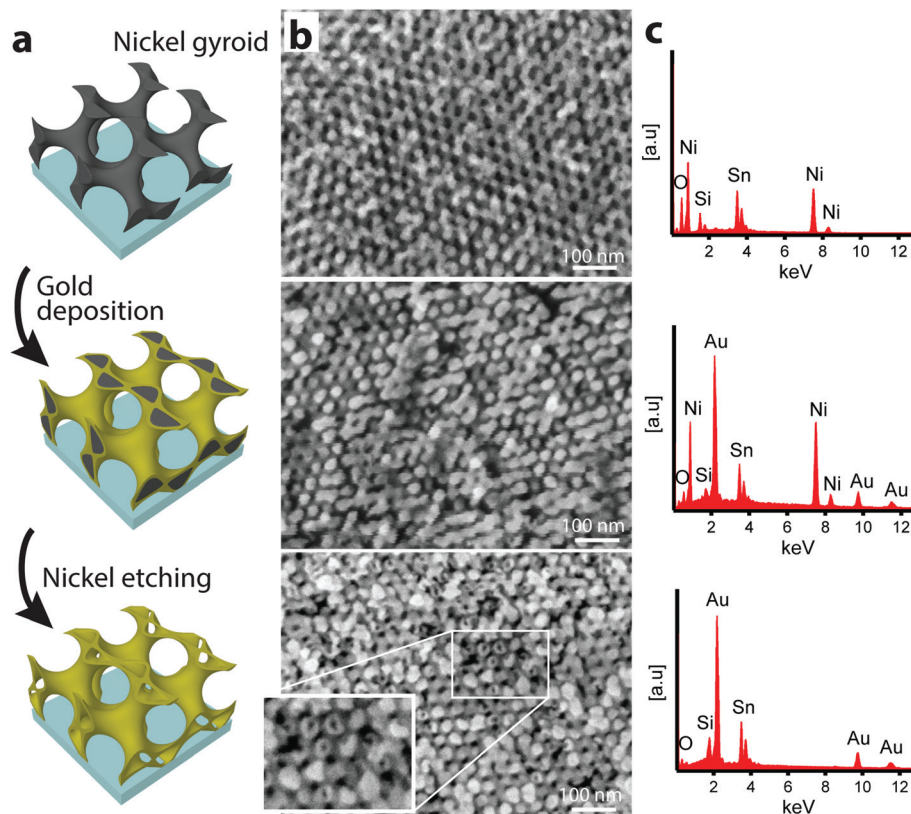


Fig. 1 Hollow gyroid manufacturing process; (a) schematic; (b) SEM micrographs; (c) EDX measurements. Top: The nickel gyroid as fabricated as described previously.¹⁵ Middle: Coating of the Ni gyroid with a thin layer of gold by electrodeposition. Bottom: Selective etching of the Ni with FeCl_3 reveals a hollow Au gyroid. The SEM images in (b, middle) show a thickening of the struts compared to (b, top) due to the Au deposition while the struts are hollow in (b, bottom) after Ni etching. This is corroborated by the EDX data showing the complete removal of Ni in (c, bottom).

used for illumination. Reflection measurements were normalized to a silver mirror reference, and transmission measurements were normalized to a FTO glass substrate.

3. Results and discussion

SEM images of the three manufacturing stages and their corresponding energy dispersive X-ray spectroscopy (EDX) results are shown in Fig. 1.

The SEM images in Fig. 1b top and middle show the homogeneous deposition of Au around the Ni struts. Despite this conformity of the gold coating, the nickel core is readily etched away by immersion in FeCl_3 , as verified by SEM and EDX in Fig. 1. This indicates that local defects and interstitial diffusion at the Au grain boundaries of the gold coating allow FeCl_3 access to the Ni-core during the etching process, without destabilising the surrounding Au-shell.

The amount of the deposited gold was measured by EDX with a quantitative accuracy of less than 1%²¹ relative to the nickel content before removal by etching. Since the amount of Ni per unit cell (fill fraction, f) is determined by the isoprene volume fraction ($\sim 30\%$) of the ISO terpolymer, the EDX elemental Au:Ni ratio in Fig. 1c middle directly determines the Au fill fraction. The EDX result in Fig. 1c bottom confirms the complete removal of the nickel core.

Reflection and transmission spectra of the coaxial hollow gyroid are compared with Au gyroids, in which Au was directly deposited onto the voided polymer matrix, similar to that in Fig. 1 top, resulting in a “full” gyroid with similar overall filling fraction. Despite nearly identical amounts of gold in the gyroid unit cell, the reflection and transmission intensities of the hollow Au gyroid are enhanced by a factor of 2 with respect to the full Au gyroid, as shown in Fig. 1.

As demonstrated before, the full Au gyroid metamaterial is characterised by a reduced gold plasma frequency¹⁵ that results in a red-shift of the plasma edge. Increasing the full gyroid filling fraction shifts the plasma edge to shorter wavelengths, approaching the value of solid Au for $f \rightarrow 1$. This is mirrored by the spectra in Fig. 2b where the inflection point of the reflection spectrum of the hollow gyroid (around 530 nm) lies at a shorter wavelength compared to the full gyroid. This is consistent with the earlier result, since for constant f the coaxial hollow gyroid has an increased outer strut radius compared to the full gyroid.

The measurement of both the transmission and reflection spectra allows us (in the absence of scattering which is small in these samples) to calculate the optical absorption shown in Fig. 2c. For constant f , absorption in the 300 nm thick hollow gyroid film is reduced by a factor of two compared to the full gyroid, yielding, according to this theory, a longer effective plasma wavelength. For constant f and lattice symmetry, the lower optical dissipation in Fig. 2c is clearly linked to the detailed Au morphology.

One of the advantages of our sample manufacture technique is the facile control of the fill-fraction; the wall width

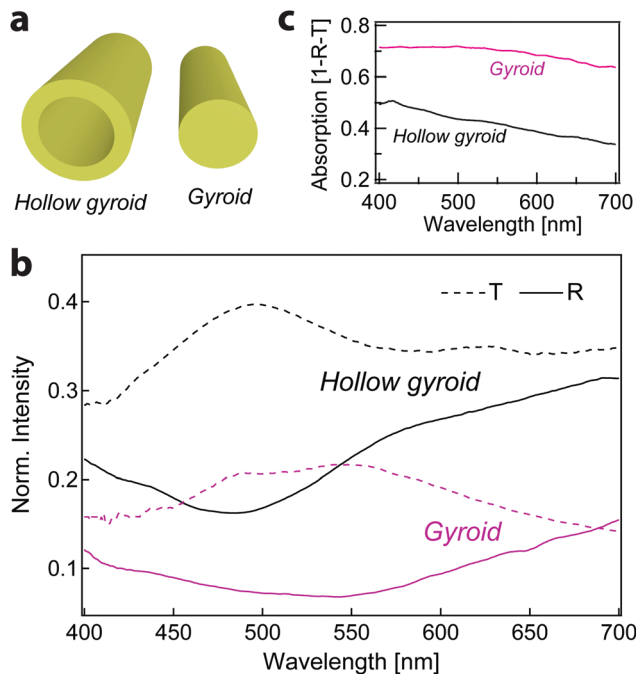


Fig. 2 (a) Schematic of the strut morphology of the coaxial hollow gyroid and full gyroid. (b) Reflection and transmission spectra of the hollow gyroid compared with the full gyroid. (c) Absorption spectra calculated from the reflection and transmission intensities. Film thickness: 300 nm, $f \approx 30\%$.

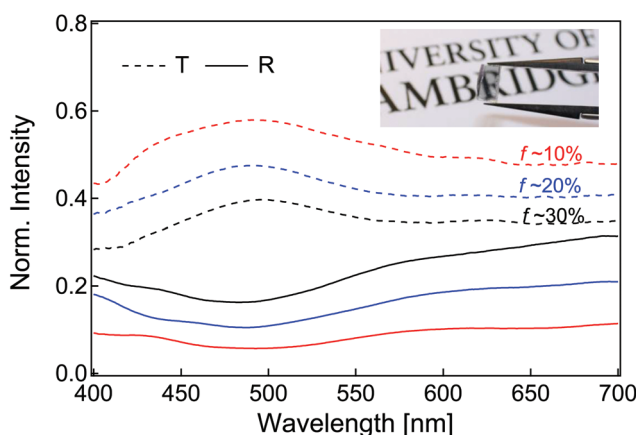


Fig. 3 Reflection and transmission spectra of hollow gyroids for filling fractions of 30%, 20% and 10%. The filling fraction was measured by EDX analysis before nickel core removal. The inset shows a photograph of the hollow gyroid with $f = 10\%$. Film thickness: 300 nm.

can simply be varied by adjusting the Au electrodeposition time. Gold filling fractions, as measured by EDX, with a Au to Ni ratio between 10% and 30%, were produced in this way. Fig. 3 establishes a clear trend: reducing f from 30% to 10% increases transmission at ≈ 500 nm from 0.4 for $f = 30\%$ to ≈ 0.48 and ≈ 0.58 for $f = 20\%$ and $f = 10\%$, respectively. Measuring the values of transmission and reflection at 500 nm yields absorptions of 0.44, 0.42 and 0.36 for f -values of 30%, 20%, and 10%, respectively.

The strut thickness of the hollow gyroid was estimated by approximating the gyroid struts as cylinders with diameters $d = 2R$ and cross-sectional areas $A = R^2\pi$. Using the 30% filling fraction per unit cell of the initial Ni struts as the reference, the added cross-sectional area of the struts upon Au plating is $A_{\text{Au}} = A_{\text{Ni}}f/0.3$. This allows us to calculate the wall thickness of the Au coating t of the hollow gyroid with equivalent fill fraction as $t_f = \pi^{-0.5}(\sqrt{A_{\text{Au}} + A_{\text{Ni}}} - \sqrt{A_{\text{Ni}}}) = R(\sqrt{1 + f/0.3} - 1)$. With the initial Ni strut diameter $d = 13$ nm, this results in $t_{30\%} \approx 2.7$ nm, $t_{20\%} \approx 1.9$ nm and $t_{10\%} \approx 1$ nm.

These results are remarkable in several ways. Starting from the same self-assembled gyroid, careful tuning of the Au composition increases transmission across a 300 nm film by nearly a factor of 3 to an unprecedented value of $\sim 60\%$, which is perhaps best visualised by the image in the inset of Fig. 3. Starting from a Ni-strut width of ≈ 13 nm, the Au-shell of the $f = 10\%$ hollow gyroid has a wall width of less than 1 nm. The structural stability of such a 3D hollow network structure is truly astounding.

While the detailed interplay of optical and plasmonic modes in the full and hollow gyroids requires extensive numerical simulations,^{13,14} the data in Fig. 2 and 3 allow a qualitative analysis. The amount of transmitted light across a film of constant thickness depends on three parameters: (1) the number of transmission modes per unit area, (2) the efficiency of in- and out-coupling into (and out of) these transmission modes, and (3) the optical absorption per mode. We expect that the hollow struts provide a wave-guide type structure that allows additional plasmon modes to propagate inside the struts, which can contribute to the overall transmission. This is rationalized by analogy with hollow nanoparticles that allow additional plasmon modes arising from the presence of the additional internal surface.²² The in- and out-coupling efficiency is very difficult to estimate even with numerical methods. How the light coupled to the structure is strongly dependent on the termination of the structure on the macroscopic surface of the material. Small differences (less than 10 nm) in the way that the unit cell of the gyroid is terminated can produce significant variations in the coupling efficiency. As this effect is true both for hollow and solid gyroids we assume to have an average response that is proportional to the number of modes if we integrate it on a sufficiently large range of frequencies. Optical absorption is clearly reduced, by a factor of about 2 when comparing the full and hollow gyroids. Since the skin-depth of Au varies between 20 and 50 nm for optical frequencies, all conduction-band electrons participate in the surface plasmon resonances that propagate along the gyroid struts. Per mode the dissipation depends on the overall thickness of the material (*i.e.* the number of electrons that participate in the oscillation and their displacement amplitude), which is clearly borne out by the data.

The changes in propagating modes and absorption alone do not however fully account for the data in Fig. 3. The morphology of these three samples is very similar, and it is unlikely that the number of propagating modes differs significantly between them. While changes in absorption from 0.44

to 0.36 are seen when going from $f = 30\%$ to $f = 10\%$ which corroborates the argument above, it accounts for only approx. 1/2 of the 18% absolute increase in transmission. In the absence of scattering, the difference has to be attributed to the reflection channel: the in-coupling of light into the $f = 10\%$ hollow gyroid is about 10% more efficient compared to the $f = 30\%$ gyroid.

Careful comparison of the 4 datasets in Fig. 2 and 3 therefore suggests that an interplay of all three mechanisms is responsible for the extraordinary transmission of light across the 300 nm thick Au metamaterial. Hollow components within metamaterials can thus cause changes in the input coupling, propagation loss, and add additional propagating modes.

4. Conclusions

In conclusion we have demonstrated a substantial transmission enhancement across an optical metamaterial based on a block copolymer self-assembled morphology. Optical transmission was increased by a factor of nearly 3 when replacing the full Au struts with hollow wave-guide morphologies. The overall transmission was shown to depend sensitively on the wall-thickness of the hollow struts, which was demonstrated down to 1 nm. Our data indicates that the dramatic transmission increase arises from an interplay of three mechanisms: (1) the additional number of modes propagating through the wave-guide structure, (2) the increased efficiency of light in-coupling, and (3) a reduction of dissipation by decreasing the Au-volume experienced in plasmon mode propagation to values much below the Au skin-depth.

These findings are likely to be useful for the design of 3D metamaterials and can pave the way to applications requiring low-loss optical metamaterials.

Acknowledgements

We acknowledge the EPSRC EP/G060649/1, the Doctoral Training Centre NanoDTC EP/G037221/1, and ERC LINASS 320503 for funding.

References

- 1 J. Pendry, *Contemp. Phys.*, 2004, **45**, 191–202.
- 2 D. Smith, J. Pendry and M. Wiltshire, *Science*, 2004, **305**, 788–792.
- 3 B. J. B. Pendry and D. R. Smith, *Sci. Am.*, 2006, 60–67.
- 4 D. R. Smith, W. J. Padilla, D. Vier, S. C. Nemat-Nasser and S. Schultz, *Phys. Rev. Lett.*, 2000, **84**, 4184.
- 5 D. Schurig, J. Mock, B. Justice, S. Cummer, J. Pendry, A. Starr and D. Smith, *Science*, 2006, **314**, 977–980.
- 6 D. Smith, W. Padilla, D. Vier, S. Nemat-Nasser and S. Schultz, *Negative permeability from split ring resonator arrays*, 2000.

- 7 T.-J. Yen, W. Padilla, N. Fang, D. Vier, D. Smith, J. Pendry, D. Basov and X. Zhang, *Science*, 2004, **303**, 1494–1496.
- 8 N. Katsarakis, G. Konstantinidis, A. Kostopoulos, R. Penciú, T. Gundogdu, M. Kafesaki, E. Economou, T. Koschny and C. Soukoulis, *Opt. Lett.*, 2005, **30**, 1348–1350.
- 9 S. Linden, C. Enkrich, M. Wegener, J. Zhou, T. Koschny and C. M. Soukoulis, *Science*, 2004, **306**, 1351–1353.
- 10 S. Zhang, W. Fan, N. Panoiu, K. Malloy, R. Osgood and S. Brueck, *Opt. Express*, 2006, **14**, 6778–6787.
- 11 S. P. Burgos, R. de Waele, A. Polman and H. A. Atwater, *Nat. Mater.*, 2010, **9**, 407–412.
- 12 D. Smith, *Science*, 2010, **327**, 138–139.
- 13 A. Demetriadou, S. S. Oh, S. Wuestner and O. Hess, *New J. Phys.*, 2012, **14**, 083032.
- 14 S. S. Oh, A. Demetriadou, S. Wuestner and O. Hess, *Adv. Mater.*, 2013, **25**(4), 612–617.
- 15 S. Vignolini, N. a. Yufa, P. S. Cunha, S. Guldin, I. Rushkin, M. Stefik, K. Hur, U. Wiesner, J. J. Baumberg and U. Steiner, *Adv. Mater.*, 2012, **24**, OP23–OP27.
- 16 S. Salvatore, A. Demetriadou, S. Vignolini, S. S. Oh, S. Wuestner, N. a. Yufa, M. Stefik, U. Wiesner, J. J. Baumberg, O. Hess and U. Steiner, *Adv. Mater.*, 2013, **25**, 2713–2716.
- 17 K. Hur, Y. Francescato, V. Giannini, S. a. Maier, R. G. Hennig and U. Wiesner, *Angew. Chem., Int. Ed.*, 2011, **50**, 11985–11989.
- 18 I. W. Hamley, *The physics of block copolymers*, Oxford University Press, New York, 1998.
- 19 P. J. Flory, *J. Chem. Phys.*, 1942, **10**, 51–61.
- 20 F. S. Bates and G. H. Fredrickson, *Phys. Today*, 1999, 32–38.
- 21 J. Goldstein, D. E. Newbury, D. C. Joy, C. E. Lyman, P. Echlin, E. Lifshin, L. Sawyer and J. R. Michael, *Scanning electron microscopy and X-ray microanalysis*, Springer, 2003.
- 22 E. Prodan and P. Nordlander, *J. Chem. Phys.*, 2004, **120**(11), 5444–5454.